INTERNATIONAL JOURNAL OF
NUMERICAL ANALYSIS AND MODELING
Volume 8, Number 2, Pages 284–301

IMMERSED FINITE ELEMENT METHODS FOR ELLIPTIC INTERFACE PROBLEMS WITH NON-HOMOGENEOUS JUMP CONDITIONS

XIAOMING HE, TAO LIN, AND YANPING LIN

Abstract. This paper is to develop immersed finite element (IFE) functions for solving second order elliptic boundary value problems with discontinuous coefficients and non-homogeneous jump conditions. These IFE functions can be formed on meshes independent of interface. Numerical examples demonstrate that these IFE functions have the usual approximation capability expected from polynomials employed. The related IFE methods based on the Galerkin formulation can be considered as natural extensions of those IFE methods in the literature developed for homogeneous jump conditions, and they can optimally solve the interface problems with a nonhomogeneous flux jump condition.

Key Words. Key words: interface problems, immersed interface, finite element, nonhomogeneous jump conditions.

1. Introduction

In this paper, we consider the following typical elliptic interface problems:

$$-\nabla \cdot \big(\beta \nabla u\big) = f(x,y),\ (x,y) \in \Omega, \tag{1.1}$$

$$u|_{\partial\Omega} = g(x,y) \tag{1.2}$$

together with the jump conditions on the interface Γ:

$$[u]\,|_{\Gamma} = 0, \tag{1.3}$$

$$\left[\beta \frac{\partial u}{\partial \mathbf{n}}\right]|_{\Gamma} = Q(x,y). \tag{1.4}$$

Here, see the sketch in Figure 1, without loss of generality, we assume that $\Omega \subset I\!R^2$ is a rectangular domain, the interface Γ is a curve separating Ω into two sub-domains Ω^-, Ω^+ such that $\overline{\Omega} = \overline{\Omega^-} \cup \overline{\Omega^+} \cup \Gamma$, and the coefficient $\beta(x,y)$ is a piecewise constant function defined by

$$\beta(x,y) = \begin{cases} \beta^-,\ (x,y) \in \Omega^-, \\ \beta^+,\ (x,y) \in \Omega^+. \end{cases}$$

Interface problem (1.1) - (1.4) appears in many applications. For example, the electric potential u satisfies jump conditions (1.3) and (1.4) on the interface between two isotropic media if the surface charge density Q on Γ is not zero [10]. Another example is the modeling of water flow in a domain consisting of two stratified porous media with a source at the interface between the media [35].

Received by the editors September 3, 2009 and, in revised form, June 25, 2010.
2000 *Mathematics Subject Classification.* 65N15, 65N30, 65N50, 35R05.
This work is partially supported by NSF grant DMS-0713763, the Research Grants Council of the Hong Kong Special Administrative Region, China (Project No. PolyU 501709) and NSERC (Canada).

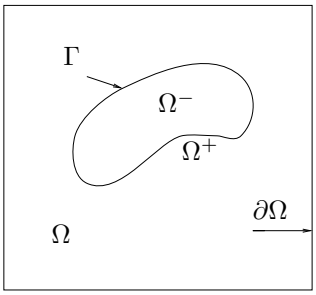

FIGURE 1. A sketch of the domain for the interface problem.

The interface problem (1.1) - (1.4) can be solved by conventional numerical methods, including both finite difference (FD) methods, see [17, 37] and references therein, and finite element (FE) methods, see [3, 6, 9] and references therein, provided that the computational meshes are body-fitting. A body-fitting mesh, see the illustration in Figure 2, is constructed according to the interface such that each element/cell in this mesh is essentially on one side of the interface. Physically, this means each element/cell in a body-fitting mesh is essentially occupied by one of the materials forming the simulation domain of the interface problem.

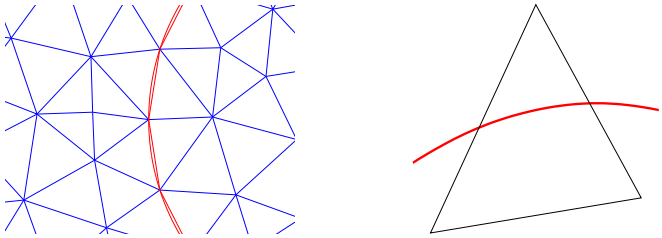

FIGURE 2. The plot on the left shows how elements are placed along an interface in a standard FE method. An element not allowed in a standard FE method is illustrated by the plot on the right.

For a non-trivial interface Γ, it is usually not possible to solve the interface problem on a structured mesh satisfactorily. On the other hand, there are applications, such as particle-in-cell simulation of plasma driven by the electric field in a Micro-Ion Thrusters [39, 40], in which it is preferable to solve the interface problem on a structured Cartesian mesh. Therefore, many efforts have been made for developing interface problem solvers that can use meshes independent of interface. In finite difference/volume formulation, we note the Cartesian grid methods [36], embedded boundary methods [18], immersed interface method [12, 20, 26, 27, 29], cut-cell methods [19, 21], matched interface and boundary methods [44, 45], etc.. In finite element formulation, Babuška et al. [4, 5] developed the generalized finite element method. Their basic idea is to form the local basis functions in an element by solving the interface problem locally. The local basis functions in their method can capture important features of the exact solution and they can even be non-polynomials. The recently developed immersed finite element (IFE) methods [1, 2, 8, 11, 13, 15, 16, 24, 25, 28, 30, 31, 32, 33, 34, 38, 41] also fall into this framework. The IFEs are developed such that their mesh can be independent of the interface, but the local basis functions are constructed according to the interface jump conditions; hence,

structured Cartesian meshes can be used to solve interface problems with non-trivial interfaces. Also, the basis functions in an IFE space are piecewise polynomials. Some other methods and related applications can be seen in [7, 22, 23, 42, 43].

However, most of the previous articles about IFE are developed for solving interface problems with the homogeneous flux jump condition. Recently, Y. Gong, B. Li and Z. Li [13] have developed an IFE method using homogenization based on the level set idea to deal with the nonhomogeneous flux jump conditions. Our goal here is to present an alternative approach by enriching the IFE spaces locally in elements cut through by interfaces. The basic idea is to locally add piecewise polynomials that can approximate the non-homogeneous flux jump condition satisfactorily. Since this new method is completely in the finite element framework, it can be easily implemented by slightly modifying the existing IFE packages.

The rest of this article is organized as follows. In Section 2, we construct IFE functions for solving interface problems with a nonhomogeneous flux jump condition. IFE functions built locally on interface elements in 1D, 2D triangular, and 2D rectangular meshes will be discussed. In Section 3, we will discuss how to form the IFE interpolation to approximate functions with a nonhomogeneous flux jump. We will demonstrate that our new IFE interpolations have the optimal convergence rate. In Section 4, we show how these IFE functions can be used in a Galerkin formulation to solve interface problems with a nonhomogeneous flux jump, and numerical examples will be presented to show the optimal convergence of these new IFE methods. Brief conclusions will be given in Section 5.

2. IFE functions for the nonhomogeneous flux jump condition

In this section we describe IFE functions that can be used to approximate functions satisfying interface jump conditions (1.3) and (1.4). IFE functions defined on the 1D, 2D triangular, and 2D rectangular meshes will be discussed. In each case, we first recall those IFE spaces capable of handling homogeneous jump conditions. Then, we will describe how to enrich these spaces locally in each interface element by adding a new IFE function that is constructed with the nonhomogeneous flux jump condition.

2.1. One dimensional IFE functions. In one dimension, the interface problem (1.1) - (1.4) becomes

$$-(\beta u')' = f,\ x \in \Omega = (a,b), \tag{2.5}$$

$$u(a) = g_l, u(b) = g_r, \tag{2.6}$$

$$[u]|_\alpha = u(\alpha+) - u(\alpha-) = 0, \tag{2.7}$$

$$[\beta u']|_\alpha = \beta^+ u'(\alpha+) - \beta^- u'(\alpha-) = Q, \tag{2.8}$$

where, without loss of generality, we have assumed that there exists only one interface $\alpha \in (a,b)$ and

$$\beta(x) = \begin{cases} \beta^-, & x \in \Omega^- = (a,\alpha), \\ \beta^+, & x \in \Omega^+ = (\alpha,b). \end{cases}$$

From now on, for any subset Λ of Ω, we let

$$\Lambda^s = \Lambda \cap \Omega^s,\ s = -,+.$$

First, we recall the 1-D linear IFE functions developed for handling the homogeneous jump conditions [28]. We refer the readers to [1, 2] for extensions to 1D higher

degree IFE functions and related analysis. We start with a mesh $\mathcal{T}_h$ of $\Omega = (a, b)$:

$$a = A_0 < A_1 < \cdots < A_i < A_{i+1} < \cdots < A_N < A_{N+1} = b,$$
$$h_j = A_{j+1} - A_j, j = 0, 1, \cdots, N, h = \max_{0 \le j \le N} h_j,$$

such that $\alpha \in (A_i, A_{i+1})$. For a typical non-interface element $T = [A_k, A_{k+1}], k = 0, 1, \cdots, N, k \neq i$, we use the usual linear finite element functions to define the local finite element space $S_h(T_k) = span\{\psi_1(x), \psi_2(x)\}$ with

$$\psi_1(x) = \frac{A_{k+1} - x}{h_k}, \ \psi_2(x) = \frac{x - A_k}{h_k}.$$

On the interface element $T = [x_i, x_{i+1}]$, we will use the IFE functions in the following form:

$$\phi(x) = \begin{cases} \phi^-(x) = a_l x + b_l, & x \in T_i^- = [A_i, \alpha], \\ \phi^-(x) = a_r x + b_r, & x \in T_i^+ = [\alpha, A_{i+1}], \\ [\phi]|_\alpha = 0, & [\beta \phi']|_\alpha = 0. \end{cases}$$

It can be shown [2] that, on the interface element, there exists a unique linear IFE function $\phi_1(x)$ such that

$$\phi_1(A_i) = 1, \phi_1(A_{i+1}) = 0.$$

Also, there exists uniquely another IFE function $\phi_2(x)$ such that

$$\phi_2(A_i) = 0, \phi_2(A_{i+1}) = 1.$$

Then we define the local IFE space on the interface element T by $S_h(T) = span\{\phi_1, \phi_2\}$.

By definition, every IFE function $v_h(x) \in S_h(\Omega)$ satisfies the homogeneous jump conditions. In order to handle the nonhomogeneous flux jump condition (2.8), we enrich the local IFE space $S_h(T)$ on the interface element T by introducing another IFE function $\phi_{T,J}(x)$ such that

$$\phi_{T,J}(x) = \begin{cases} c^-(x - x_i), & x \in T_i^- \\ c^+(x_{i+1} - x), & x \in T_i^+, \\ [\phi_{T,J}]|_\alpha = 0, & [\beta \phi'_{T,J}]|_\alpha = 1. \end{cases} \tag{2.9}$$

By straightforward calculations, we can see that

$$\phi_{T,J}(x_i) = \phi_{T,J}(x_{i+1}) = 0$$

and the coefficients c^- and c^+ can be uniquely determined as follows:

$$c^- = \frac{A_{i+1} - \alpha}{\beta^-(\alpha - A_{i+1}) + \beta^+(A_i - \alpha)}, \tag{2.10}$$

$$c^+ = \frac{A_i - \alpha}{\beta^-(\alpha - A_{i+1}) + \beta^+(A_i - \alpha)}. \tag{2.11}$$

See Figure 3 for a sketch of $\phi_{T,J}(x)$ where $T = [-1, 1], \beta^- = 1, \beta^+ = 2$, and $\alpha = \pi/6$.

2.2. Two dimensional triangular IFE functions. We now consider triangular IFE functions for solving the 2-D interface problem (1.1) - (1.4). First, we introduce a typical triangular mesh $\mathcal{T}_h$ on Ω that is independent of the interface Γ. When the mesh size is small enough, only a few elements in $\mathcal{T}_h$ are cut through by the interface Γ and we call them the interface elements. Most of the element are non-interface elements. Without loss of generality, we assume in the discussion from now on that the mesh $\mathcal{T}_h$ has the following features when the mesh size is small enough:

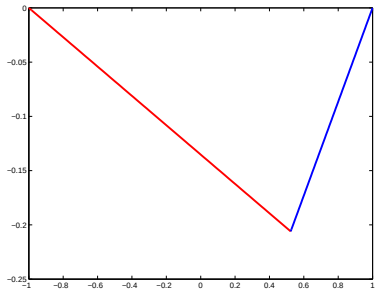

FIGURE 3. The 1D linear IFE function dealing with the non-homogeneous flux jump condition on the reference element with $\beta^- = 1, \beta^+ = 2, \alpha = \pi/6$.

(H_1): The interface Γ will not intersect an edge of any element at more than two points unless this edge is part of Γ.

(H_2): If Γ intersects the boundary of an element at two points, then these two points must be on different edges of this element.

On a typical non-interface element $T = \triangle A_1A_2A_3$, we use the usual local linear finite element space $S_h(T) = span\{\psi_i(x,y), i = 1,2,3\}$ with linear polynomials such that

$$\psi_i(A_j) = \begin{cases} 1, & \text{if } i = j \\ 0, & \text{if } i \neq j. \end{cases} \tag{2.12}$$

Note that linear polynomials are universal, they have no direct relationship with the interface problems to be solved. Hence, on each interface element, we will use the IFE functions that can partially solve the interface problems in a certain sense. To describe these IFE functions on a typical interface element $T = \triangle A_1A_2A_3$, we assume that the interface Γ intersect the boundary of T at points D and E. The line $\overline{DE}$ separates T into two sub-elements $\tilde{T}^-$ and $\tilde{T}^+$, see the illustration in Figure 4. As in the 1-D case, we will introduce two groups of IFE functions on T. The first group of IFE functions can represent functions values at the vertices of T and the second group are for representing the non-zero flux jump. The IFE functions in the first group are those introduced in [31, 32] characterized by the following formulas:

$$\phi(x,y) = \begin{cases} \phi^-(x,y) = a^-x + b^-y + c^-, & (x,y) \in \tilde{T}^-, \\ \phi^+(x,y) = a^+x + b^+y + c^+, & (x,y) \in \tilde{T}^+, \\ \phi^-(D) = \phi^+(D),\ \phi^-(E) = \phi^+(E), & \\ \beta^+ \dfrac{\partial \phi^+}{\partial \mathbf{n}_{\overline{DE}}} - \beta^- \dfrac{\partial \phi^-}{\partial \mathbf{n}_{\overline{DE}}} = 0, & \end{cases} \tag{2.13}$$

where $\mathbf{n}_{\overline{DE}}$ is the unit vector perpendicular to the line $\overline{DE}$. It has been shown [31] that functions defined by (2.13) can satisfy the homogeneous flux jump condition across the interface Γ exactly in a weak sense as follows:

$$\int_{\Gamma \cap T} \left(\beta^- \frac{\partial \phi^-}{\partial \mathbf{n}_\Gamma} - \beta^+ \frac{\partial \phi^+}{\partial \mathbf{n}_\Gamma} \right) ds = 0.$$

In addition, it has been shown [31, 32] that, for each each $i = 1,2,3$, there exists a unique triangular IFE function $\phi_i(x,y)$ such that

$$\phi_i(A_j) = \begin{cases} 1, & \text{if } i = j, \\ 0, & \text{if } i \neq j, \end{cases} \tag{2.14}$$

and we call them the local nodal linear IFE basis functions on an interface element T. We then use these nodal basis functions to defined the local IFE space $S_h(T) = span\{\phi_1, \phi_2, \phi_3\}$.

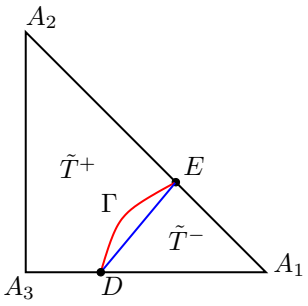

FIGURE 4. A typical triangular interface elements.

To handle the non-zero flux jump condition on an interface element T, we introduce another IFE function $\phi_{T,J}(x,y)$ that is zero at all the vertices of T but it can satisfy the unit flux jump condition. Here, we will describe the construction of $\phi_{T,J}(x,y)$ for the case in which the interface point D is on $\overline{A_1A_3}$, E is on $\overline{A_1A_2}$, see Figure 4, other cases can be handle similarly. First, the nodal value configuration suggests that

$$\phi_{T,J}(x,y) = \begin{cases} \phi^-_{T,J}(x,y) = c_2\psi_2(x,y) + c_3\psi_3(x,y), & (x,y) \in \tilde{T}^-, \\ \phi^+_{T,J}(x,y) = c_1\psi_1(x,y), & (x,y) \in \tilde{T}^+ \end{cases} \tag{2.15}$$

with coefficients $c_i, i = 1,2,3$ to be determined by the following interface jump conditions:

$$\phi^-_{T,J}(D) = \phi^+_{T,J}(D),\ \phi^-_{T,J}(E) = \phi^+_{T,J}(E), \tag{2.16}$$

$$\beta^+ \frac{\partial \phi^+_{T,J}}{\partial \mathbf{n}_{\overline{DE}}} - \beta^- \frac{\partial \phi^-_{T,J}}{\partial \mathbf{n}_{\overline{DE}}} = 1. \tag{2.17}$$

Here, $\mathbf{n}_{\overline{DE}}$ is the unit vector perpendicular to $\overline{DE}$ pointing to the same direction of the outer normal vector of $\Gamma \cap T$.

To describe the computation of $c_i, i = 1,2,3$, we turn to reference element $\hat{T} = \triangle \hat{A}_1\hat{A}_2\hat{A}_3$ with

$$\hat{A}_1 = (0,0), \hat{A}_2 = (1,0), \hat{A}_3 = (0,1).$$

We can describe $\phi_{T,J}(x,y)$ by a function $\hat{\phi}_J(\hat{x},\hat{y})$ defined on the reference element $\hat{T}$ such that

$$\phi_{T,J}(X) = \hat{\phi}_{T,J}(\hat{X}) = \hat{\phi}_{T,J}(B^{-1}(X - A_1)),$$

where B is the matrix used in the usual affine mapping between T and $\hat{T}$

$$F : \hat{T} \longrightarrow T,$$
$$F\hat{\mathbf{x}} = B\hat{\mathbf{x}} + A_1 = [A_2 - A_1, A_3 - A_1]\hat{\mathbf{x}} + A_1.$$

Through this affine mapping, we can see that (2.15) - (2.17) lead to

$$\hat{\phi}_{T,J}(\hat{x},\hat{y}) = \begin{cases} \hat{\phi}^-_{T,J}(\hat{x},\hat{y}) = c_2\hat{\psi}_2(\hat{x},\hat{y}) + c_3\hat{\psi}_3(\hat{x},\hat{y}), & (\hat{x},\hat{y}) \in \hat{\tilde{T}}^-, \\ \hat{\phi}^+_{T,J}(\hat{x},\hat{y}) = c_1\hat{\psi}_1(\hat{x},\hat{y}), & (\hat{x},\hat{y}) \in \hat{\tilde{T}}^+ \end{cases} \tag{2.18}$$

and

$$\hat{\phi}^-_{T,J}(\hat{D}) = \hat{\phi}^+_{T,J}(\hat{D}),\ \hat{\phi}^-_{T,J}(\hat{E}) = \hat{\phi}^+_{T,J}(\hat{E}), \tag{2.19}$$

$$\beta^+ \frac{\partial \hat{\phi}^+}{\partial \hat{\mathbf{n}}} - \beta^- \frac{\partial \hat{\phi}^-}{\partial \hat{\mathbf{n}}} = 1, \tag{2.20}$$

where

$$\hat{D} = F^{-1}(D) = (0, \hat{d})^t,\ \hat{E} = F^{-1}(E) = (\hat{e}, 0)^t,$$
$$(\hat{n}_1, \hat{n}_2)^t = \hat{\mathbf{n}} = B^{-1}\mathbf{n}_{\overline{DE}},\ \hat{\tilde{T}}^s = F^{-t}(\tilde{T}^s),\ s = \pm.$$

Solving the linear system (2.19) and (2.20), we obtain

$$c_1 = \frac{\hat{d}\hat{e}}{\Lambda}, c_2 = \frac{\hat{d}(1-\hat{e})}{\Lambda},\ c_3 = \frac{\hat{e}(1-\hat{d})}{\Lambda},$$
$$\Lambda = -\beta^+(\hat{n}_1 + \hat{n}_2)\hat{d}\hat{e} + \beta^-(\hat{n}_1\hat{d}(-1+\hat{e}) + \hat{n}_2\hat{e}(-1+\hat{d})).$$

It can be shown that, on an interface element T, the IFE function $\phi_{T,J}$ defined in (2.15) is uniquely determined by (2.16) and (2.17). The IFE function $\hat{\phi}_{T,J}$ is illustrated in Figure 5.

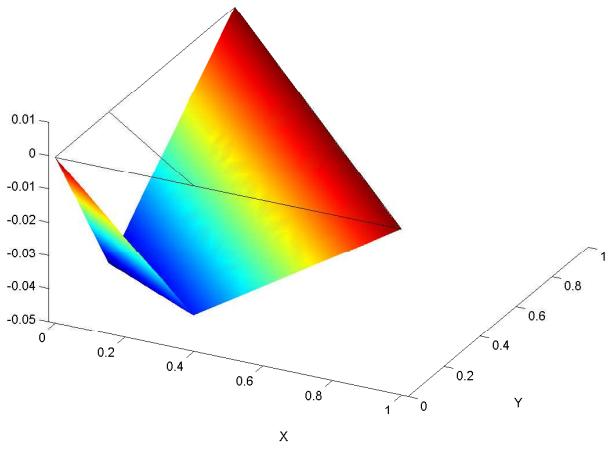

FIGURE 5. The 2D triangular IFE function dealing with the non-homogeneous flux jump condition on the reference element with $\beta^- = 1, \beta^+ = 20, D = (0, 0.3)^t, E = (0.4, 0)^t$.

2.3. Two dimensional bilinear IFE functions. Now, let $\mathcal{T}_h, h > 0$ be a family of rectangular meshes of the solution domain Ω that can be a union of rectangles. There are two types of rectangle interface elements in a mesh $\mathcal{T}_h$. Type I are those for which the interface intersects with two of its adjacent edges; Type II are those for which the interface intersects with two of its opposite edges, see the sketches in Figure 6.

As usual, on a non-interface element $T = \square A_1A_2A_3A_4$, we will use the bilinear finite element space $S_h(T) = span\{\psi_i, 1, 2, 3, 4\}$, where $\phi_i, i = 1, 2, 3, 4$ are the standard bilinear local nodal basis functions associated with the vertices of T.

Our main concern is the finite element functions in an interface element $T \in \mathcal{T}_h$. Assume that the four vertices of T are $A_i, i = 1, 2, 3, 4$, with $A_i = (x_i, y_i)^t$, and we use $D = (x_{_D}, y_{_D})^T$ and $E = (x_{_E}, y_{_E})^T$ to denote the interface points on its edges.

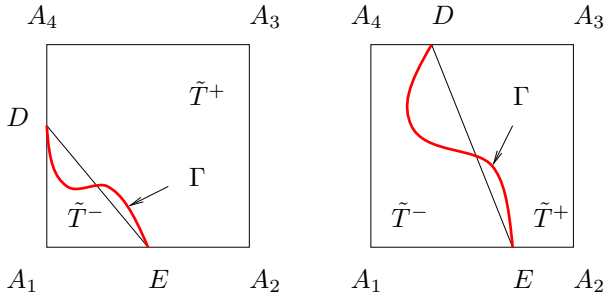

FIGURE 6. Two typical interface elements. The element on the left is of Type I while the one on the right is of Type II.

Note that the line $\overline{DE}$ separates T into two subelements: $\tilde{T}^-$ and $\tilde{T}^+$. Here $\tilde{T}^-$ is the polygon contained in T sharing at least one vertex of $\tilde{T}^-$ inside Ω^- and the other subelement is $\tilde{T}^+$. The bilinear IFE functions on T are then formed as piecewise bilinear polynomials according to $\tilde{T}^-$ and $\tilde{T}^+$ that can satisfy the interface jump conditions in a certain sense. Specifically, we will use the bilinear IFE functions discussed in [14, 15, 16, 33] on an interface element T with the following formulation:

$$\phi(x,y) = \begin{cases} \phi^-(x,y) = a^-x + b^-y + c^- + d^-xy, & (x,y) \in \tilde{T}^-, \\ \phi^+(x,y) = a^+x + b^+y + c^+ + d^+xy, & (x,y) \in \tilde{T}^+, \\ \phi^-(D) = \phi^+(D),\ \phi^-(E) = \phi^+(E),\ d^- = d^+, & \\ \int_{\overline{DE}} \left(\beta^+ \dfrac{\partial \phi^+}{\partial \mathbf{n}_{\overline{DE}}} - \beta^- \dfrac{\partial \phi^-}{\partial \mathbf{n}_{\overline{DE}}} \right) ds = 0. & \end{cases} \tag{2.21}$$

We let $\phi_i(X)$ be the IFE function described by (2.21) such that

$$\phi_i(x_j, y_j) = \begin{cases} 1, & \text{if } i = j, \\ 0, & \text{if } i \neq j, \end{cases}$$

for $1 \leq i, j \leq 4$, and we call them the bilinear IFE nodal basis functions on an interface element T. Then, we define the local bilinear IFE space on an interface element T by $S_h(T) = span\{\phi_i, i = 1, 2, 3, 4\}$.

On each interface element T, we extend the local bilinear IFE space $S_h(T)$ by adding another bilinear IFE function that can capture the non-homogeneous flux jump in a weak sense. In general, this new IFE function can be described as follows:

$$\phi_{T,J}(x,y) = \begin{cases} \phi^-_{T,J}(x,y) = a^-x + b^-y + c^- + d^-xy, & (x,y) \in \tilde{T}^-, \\ \phi^+_{T,J}(x,y) = a^+x + b^+y + c^+ + d^+xy, & (x,y) \in \tilde{T}^+, \\ \phi_{T,J}(x_j, y_j) = 0,\ j = 1, 2, 3, 4, & \\ \phi^-_{T,J}(D) = \phi^+_{T,J}(D),\ \phi^-_{T,J}(E) = \phi^+_{T,J}(E), & \\ d^- = d^+, & \\ \int_{\overline{DE}} \left(\beta^+ \dfrac{\partial \phi^+_{T,J}}{\partial \mathbf{n}_{\overline{DE}}} - \beta^- \dfrac{\partial \phi^-_{T,J}}{\partial \mathbf{n}_{\overline{DE}}} \right) ds = 1. & \end{cases} \tag{2.22}$$

Because (2.22) leads to a linear system whose coefficient matrix is the same as that in the linear system defining ϕ_i in (2.21), the existence and uniqueness of $\phi_{T,J}$ are equivalent to those of ϕ_i, which have been showed in [14, 15, 33].

On the other hand, the zero nodal values lead to a simpler determination of $\phi_{T,J}$ than solving for 8 coefficients $a^\pm, b^\pm, c^\pm, d^\pm$ directly from the linear system described in (2.22). To see this, let us consider a Type I interface element as sketched

in Figure 6, other cases can be discussed similarly. In this case, $\phi_{T,J}$ can be equivalently rewritten as follows

$$\phi_{T,J}(x,y) = \begin{cases} \phi^-_{T,J}(x,y) = c_2\psi_2(x,y) + c_3\psi_3(x,y) + c_4\psi_4(x,y), & (x,y) \in \tilde{T}^-, \\ \phi^+_{T,J}(x,y) = c_1\psi_1(x,y), & (x,y) \in \tilde{T}^+, \\ \phi^-_{T,J}(D) = \phi^+_{T,J}(D),\ \phi^-_{T,J}(E) = \phi^+_{T,J}(E), \\ \dfrac{\partial^2\phi^-_{T,J}}{\partial x\partial y} = \dfrac{\partial^2\phi^+_{T,J}}{\partial x\partial y}, \\ \int_{\overline{DE}} \left(\beta^+ \dfrac{\partial\phi^+_{T,J}}{\partial \mathbf{n}_{\overline{DE}}} - \beta^- \dfrac{\partial\phi^-_{T,J}}{\partial \mathbf{n}_{\overline{DE}}} \right) ds = 1, \end{cases}$$

where $\psi_i,\ i = 1,2,3,4$ are the standard bilinear finite element nodal basis functions at $A_i,\ i = 1,2,3,4$, and $\mathbf{n}_{\overline{DE}}$ has the same meaning as in the triangular case covered in the previous subsection. This means that $\phi_{T,J}$ is actually determined by 4 coefficients $c_i, i = 1,2,3,4$.

Following a procedure similar to the one used for the triangular interface elements, we can compute $c_i, i = 1,2,3,4$ on the reference element $\hat{T}$ with vertices $\hat{A}_i = (\hat{x}_i, \hat{y}_i)^T, i = 1,2,3,4$ such that

$$\hat{A}_1 = \begin{pmatrix} 0 \\ 0 \end{pmatrix}, \hat{A}_2 = \begin{pmatrix} 1 \\ 0 \end{pmatrix}, \hat{A}_3 = \begin{pmatrix} 1 \\ 1 \end{pmatrix}, \hat{A}_4 = \begin{pmatrix} 0 \\ 1 \end{pmatrix}.$$

Using the usual affine mapping:

$$X = F(\hat{X}) = A_1 + B\hat{X},\ B = (A_2 - A_1, A_4 - A_1),\ X = \begin{pmatrix} x \\ y \end{pmatrix},\ \hat{X} = \begin{pmatrix} \hat{x} \\ \hat{y} \end{pmatrix}.$$

we define

$$\hat{\phi}_{T,J}(\hat{X}) = \hat{\phi}_{T,J}(B^{-1}(X - A_1)) = \phi_{T,J}(X).$$

Note that through this affine mapping D and E become

$$\hat{D} = F^{-1}(D) = \begin{pmatrix} 0 \\ \hat{b} \end{pmatrix}, \hat{E} = F^{-1}(E) = \begin{pmatrix} \hat{a} \\ 0 \end{pmatrix}$$

and $\overline{\hat{D}\hat{E}}$ separates $\hat{T}$ into $\hat{\tilde{T}}^+$ and $\hat{\tilde{T}}^-$. Suppose the local interface element has size $h \times h$. Then (2.23) leads to

$$\hat{\phi}_{T,J}(\hat{x},\hat{y}) = \begin{cases} \hat{\phi}^-_{T,J}(\hat{x},\hat{y}) = c_2\hat{\psi}_2(\hat{x},\hat{y}) + c_3\hat{\psi}_3(\hat{x},\hat{y}) + c_4\hat{\psi}_4(\hat{x},\hat{y}), & (\hat{x},\hat{y}) \in \hat{\tilde{T}}^-, \\ \hat{\phi}^+_{T,J}(\hat{x},\hat{y}) = c_1\hat{\psi}_1(\hat{x},\hat{y}), & (\hat{x},\hat{y}) \in \hat{\tilde{T}}^+, \\ \hat{\phi}^-_{T,J}(\hat{D}) = \hat{\phi}^+_{T,J}(\hat{D}),\ \hat{\phi}^-_{T,J}(\hat{E}) = \hat{\phi}^+_{T,J}(\hat{E}), \\ \dfrac{\partial^2\hat{\phi}^-_{T,J}}{\partial\hat{x}\partial\hat{y}} = \dfrac{\partial^2\hat{\phi}^+_{T,J}}{\partial\hat{x}\partial\hat{y}}, \\ \int_{\overline{\hat{D}\hat{E}}} \left(\beta^+ \dfrac{\partial\hat{\phi}^+_{T,J}}{\partial\hat{\mathbf{n}}} - \beta^- \dfrac{\partial\hat{\phi}^-_{T,J}}{\partial\hat{\mathbf{n}}} \right) h d\hat{s} = 1. \end{cases}$$

Here $\hat{\psi}_i, i = 1,2,3,4$ are the four standard bilinear finite element nodal basis functions associated with $\hat{A}_i, i = 1,2,3,4$ and $\hat{\mathbf{n}} = (\hat{n}_1, \hat{n}_2)^t = B^{-1}\mathbf{n}_{\overline{DE}}$. Solving the linear system defined by (2.23), we obtain the following formulas for $c_i, i = 1,2,3,4$:

$$c_1 = \frac{2\hat{a}\hat{b}}{\Lambda},\ c_2 = \frac{2\hat{b}(1-\hat{a})}{\Lambda},\ c_3 = \frac{2(\hat{a}+\hat{b}-\hat{a}\hat{b})}{\Lambda},\ c_4 = \frac{2\hat{a}(1-\hat{b})}{\Lambda},$$

$$\Lambda = h\sqrt{(\hat{a}^2+\hat{b}^2)}(-2\beta^-\hat{a}\hat{n}_2 + 2\beta^-\hat{a}\hat{n}_2\hat{b} - 2\beta^-\hat{b}\hat{n}_1 + 2\beta^-\hat{b}\hat{n}_1\hat{a} + \beta^+\hat{b}^2\hat{n}_1\hat{a} + \beta^+\hat{a}^2\hat{n}_2\hat{b} - 2\beta^+\hat{b}\hat{n}_1\hat{a} - 2\beta^+\hat{a}\hat{n}_2\hat{b} - \beta^-\hat{b}^2\hat{n}_1\hat{a} - \beta^-\hat{a}^2\hat{n}_2\hat{b}).$$

See Figure 7 for sketches of the two typical bilinear IFE functions of Type I and Type II for the nonhomogeneous flux jump condition.

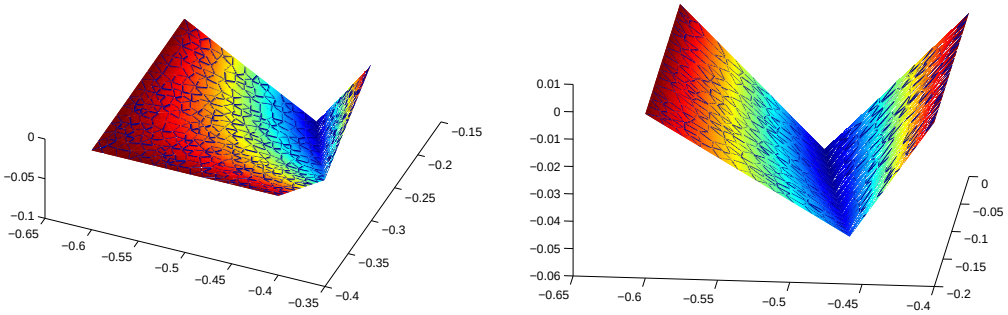

FIGURE 7. The plot on the left is a ϕ_J on a Type I interface element and the plot on the right is a ϕ_J on a Type II interface element.

3. Approximation capability of the IFE functions

In this section, we discuss how to use the new IFEs to approximate continuous functions that have a nonhomogeneous flux jump across the interface. We will present numerical results to demonstrate the optimal approximation capability of these IFE functions from the point of view of the polynomials employed. Following notation will be used in the description of the IFE interpolation: for a given set $\Lambda \subset \Omega$, we let

$$PH^2_{int}(\Lambda) = \left\{ u \in C(T), u|_{\Lambda^s} \in H^2(\Lambda^s), s = -, +, \left[\beta \frac{\partial u}{\partial \mathbf{n}_\Gamma}\right] = Q \text{ on } \Gamma \cap \Lambda \right\}.$$

First, for a given continuous function u, we construct the interpolation with these IFE functions locally on each element T in a mesh $\mathcal{T}_h$. If T is a non-interface element, we define the interpolation of u on T as:

$$I_{h,T}u(X) = \sum_{i=1}^{N_T} u(A_i)\psi_i(X),$$

where

$$X = \begin{cases} x, & \text{if } T \text{ is a 1D element,} \\ (x, y), & \text{if } T \text{ is a 2D element,} \end{cases}$$

$$N_T = \begin{cases} 2, & \text{if } T \text{ is an 1D element,} \\ 3, & \text{if } T \text{ is a 2D triangular element,} \\ 4, & \text{if } T \text{ is a 2D rectangular element,} \end{cases}$$

and $\psi_i, 1 \le i \le N_T$ are the standard linear or bilinear local nodal basis functions on T.

On an interface element $T \in \mathcal{T}_h$, assuming that u is in $PH^2_{int}(T)$, we define the IFE interpolation of u by

$$I_{h,T}u(X) = \sum_{i=1}^{N_T} u(A_i)\phi_i(X) + q_T\phi_{T,J}(X),$$

where $\phi_i, 1 \le i \le N_T$ are the local nodal IFE functions on T with a homogeneous flux jump discussed in the previous section, and $\phi_{T,J}(X)$ is the new IFE function with a unit flux jump in a certain sense. We also have the following choices for the interpolation parameter q_T:

$$q_T = \begin{cases} Q, & \text{if } T \text{ is an 1D interface element,} \\ \dfrac{\int_{\Gamma\cap T} Q ds}{\left|\overline{DE}\right|}, & \text{if } T \text{ is a 2D triangular interface element,} \\ \int_{\Gamma\cap T} Q ds, & \text{if } T \text{ is a 2D rectangular interface element.} \end{cases} \tag{3.23}$$

Accordingly, for a function $u \in PH^2_{int}(\Omega)$, we let $I_h u$ be its interpolation such that $I_h u|_T = I_{h,T}(u|_T)$ for any $T \in \mathcal{T}_h$. Using the properties of the local IFE functions, we can show that the IFE function $I_h u$ on an interface element T has the following features:

- $I_{h,T}u(A_i) = u(A_i), 1 \le i \le N_T$ and this implies $I_{h,T}u(X)$ interpolates $u(X)$ on T.
- In the 1D case, $I_{h,T}u$ is in $PH^2_{int}(T)$, i.e., $I_{h,T}u$ can exactly satisfy the interface jump conditions.
- In the 2D case, $[I_{h,T}u]_{\overline{DE}} = 0$ which implies that $I_{h,T}u \in C^0(T)$ and $I_{h,T}u$ locally satisfies interface jump condition (1.3).
- In the 2D case, $I_h u$ can also satisfy the flux jump condition (1.4) exactly in the following weak sense:

$$\int_{\Gamma\cap T} \left[\beta \frac{\partial I_{h,T}u}{\partial \mathbf{n}}\right] ds = \int_{\Gamma\cap T} Q ds.$$

All of these properties suggest that $I_h u$ should be a reasonable approximation to u. We now use numerical examples to demonstrate that $I_h u$ can approximate u with an optimal convergence rate provided that u have enough piecewise smoothness.

1D IFE interpolation: We consider a function

$$u(x) = \begin{cases} e^x, & x \in [0, \alpha], \\ sin((x-\alpha)) + e^\alpha, & x \in [\alpha, 1] \end{cases} \tag{3.24}$$

with

$$\beta^- = 1, \beta^+ = 20000, \alpha = \pi/6.$$

By simple calculations we can see that u satisfies the following jump conditions at α:

$$[u]|_\alpha = 0,\ \beta^+ u'(\alpha+) - \beta^- u'(\alpha-) = 20000 - e^\alpha.$$

The errors of $I_h u$ in the L^2 and the semi-H^1 norms are listed in Table 1. Applying linear regression on the datum in this table, we have

$$\|I_h u - u\|_0 \approx 7.7584 \times 10^{-2} h^{1.9916},\ |I_h u - u|_1 \approx 2.7160 \times 10^{-1} h^{0.9934}.$$

which clearly demonstrate the optimal approximation capability of $I_h u$ because $I_h u$ is a piecewise linear polynomial.

h	$\|I_h u - u\|_0$	$\|I_h u - u\|_1$
1/16	3.0784×10^{-4}	1.7139×10^{-2}
1/32	7.7837×10^{-5}	8.7038×10^{-3}
1/64	1.9706×10^{-5}	4.3791×10^{-3}
1/128	4.9804×10^{-6}	2.2083×10^{-3}
1/256	1.2451×10^{-6}	1.1042×10^{-3}
1/512	3.1128×10^{-7}	5.5208×10^{-4}
1/1024	7.7819×10^{-8}	2.7604×10^{-4}

TABLE 1. Errors in the 1D linear IFE interpolation $I_h u$ with $\beta^- = 1$ and $\beta^+ = 20000$.

2D triangular IFE interpolation: In this example, we use the following function to demonstrate the approximation capability of the triangular IFE functions:

$$u(x,y) = \begin{cases} \dfrac{(x^2+y^2)^{\alpha/2}}{\beta^-}, & (x,y) \in \Omega^-, \\ \dfrac{(x^2+y^2)^{\alpha/2}}{\beta^+} + \left(\dfrac{1}{\beta^-} - \dfrac{1}{\beta^+}\right) r_0^\alpha & \\ +\delta(\sqrt{x^2+y^2} - r_0), & (x,y) \in \Omega^+, \end{cases} \tag{3.25}$$

where $\alpha = 3, r_0 = \pi/6.28, \delta = 10, \Omega = (-1,1) \times (-1,1)$,

$$\Omega^- = \{(x,y)^t \in I\!R^2 \mid x^2 + y^2 < r_0^2\}$$

and $\Omega^+ = \Omega \backslash \Omega^-$. The coefficient β is

$$\beta(x,y) = \begin{cases} \beta^- = 10000, & (x,y) \in \Omega^-, \\ \beta^+ = 10, & (x,y) \in \Omega^+, \end{cases}$$

which is discontinuous across the interface

$$\Gamma = \{(x,y)^t \in I\!R^2 \mid x^2 + y^2 = r_0^2\}.$$

Note that $u(x,y)$ satisfies the following jump conditions:

$$[u]_\Gamma = 0, \ \left[\beta \frac{\partial u}{\partial \mathbf{n}}\right]_\Gamma = \delta \beta^+ = 100.$$

The errors of $I_h u$ in the L^2 and semi-H^1 norms are listed in Table 2. To generate datum in this table, we use a Cartesian mesh $\mathcal{T}_h$ for each h that is formed by partitioning Ω with rectangles of size $h \times h$, and then cutting each rectangle into two triangles along a diagonal line. Using the linear regression, we can see that the datum in this table obey

$$\|I_h u - u\|_0 \approx 2.2694 \ h^{1.9992}$$
$$|I_h u - u|_1 \approx 7.4239 \ h^{1.0008}$$

which indicate that $I_h u$ can converge to u optimally in either the L^2 norm or the semi-H^1 norm.

2D rectangular IFE interpolation: In this example, the domains Ω, Ω^- and Ω^+, and the interface Γ are the same as in the previous example. The function to be interpolated is

$$u(x,y) = \frac{(x^2+y^2)^{5/2}}{\beta^-}. \tag{3.26}$$

h	$\|I_h u - u\|_0$	$\|I_h u - u\|_1$
1/16	8.8806×10^{-3}	4.6305×10^{-1}
1/32	2.2228×10^{-3}	2.3144×10^{-1}
1/64	5.5590×10^{-4}	1.1557×10^{-1}
1/128	1.3903×10^{-4}	5.7778×10^{-2}
1/256	3.4767×10^{-5}	2.8884×10^{-2}

TABLE 2. Errors in the 2D triangular IFE interpolation $I_h u$ with $\beta^- = 10000$ and $\beta^+ = 10$.

We note that $u(x, y)$ satisfies the following jump conditions across the interface Γ:

$$[u]_\Gamma = 0, \ \left[\beta \frac{\partial u}{\partial \mathbf{n}}\right] = Q(x, y) = 5(\beta^+ - \beta^-)\frac{(x^2 + y^2)^{5/2}}{r_0}.$$

One important feature of this example is that the flux jump across the interface is not a constant function. Table 3 contains actual errors of the IFE interpolation $I_h u$ with various partition sizes h for $\beta^- = 1, \beta^+ = 10$. Using linear regression, we can also see that the datum in this table obey

$$\|I_h u - u\|_0 \approx 3.6279 \ h^{1.9998}, |I_h u - u|_1 \approx 8.7742 \ h^{0.9998},$$

which clearly indicate that the bilinear IFE interpolation $I_h u$ converges to u with the optimal convergence rates $O(h^2)$ and $O(h)$ in the L^2 norm and H^1 norm, respectively.

h	$\|I_h u - u\|_0$	$\|I_h u - u\|_1$
1/16	1.4172×10^{-2}	5.4838×10^{-1}
1/32	3.5460×10^{-3}	2.7443×10^{-1}
1/64	8.8666×10^{-4}	1.3724×10^{-1}
1/128	2.2167×10^{-4}	6.8620×10^{-2}
1/256	5.5418×10^{-5}	3.4310×10^{-2}

TABLE 3. Errors in the 2D bilinear IFE interpolation $I_h u$ with $\beta^- = 1$ and $\beta^+ = 10$.

4. IFE methods for problems with nonhomogeneous flux jump

Our numerical examples in the previous section demonstrate that the new IFE functions can optimally approximate a piecewise smooth functions with a nonhomogeneous flux jump condition across the interface. In this section, we describe how to use these IFE functions to solve the interface problems with a non-homogeneous flux jump condition.

First, we multiply the differential equation (1.1) by any $v \in H_0^1(\Omega)$ and integrate it over $\Omega^s (s = +, -)$ to have

$$-\int_{\Omega^s} \nabla \cdot (\beta^s \nabla u) v \ dxdy \quad = \quad \int_{\Omega^s} fv \ dxdy, \forall \ v \in H_0^1(\Omega).$$

Then a straightforward application of the Green's formula leads to

$$\int_{\Omega^s} \beta^s \nabla u \cdot \nabla v \ dxdy - \int_{\partial\Omega^s} \beta \frac{\partial u}{\partial \mathbf{n}} v \ ds \quad = \quad \int_{\Omega^s} fv \ dxdy, \ s = +, -, \forall \ v \in H_0^1(\Omega).$$

Summing the above equation over s, we obtain a weak formulation for the interface problem:

$$\int_\Omega \beta \nabla u \cdot \nabla v \; dxdy = \int_\Omega fv \; dxdy - \int_\Gamma Qvds, \forall \; v \in H_0^1(\Omega). \tag{4.27}$$

Here we have used the flux jump condition (1.4) and the fact that $v \in H_0^1(\Omega)$. Also, we have assumed

$$Q = \beta^+ \frac{\partial u}{\partial \mathbf{n}}|_{\Omega^+ \cap \Gamma} - \beta^- \frac{\partial u}{\partial \mathbf{n}}|_{\Omega^- \cap \Gamma}$$

with $\mathbf{n}$ being the unit normal vector of Γ pointing from Ω^- to Ω^+.

To describe the IFE solution for the interface problem, we start with a mesh $\mathcal{T}_h$ of the solution domain Ω, and let

$$\begin{aligned}
&\mathcal{N}_h = \{(x_i, y_i)^t \in I\!R^2 \mid (x_i, y_i)^t \text{ is a node of } \mathcal{T}_h\},\\
&\mathcal{N}_h^o = \mathcal{N}_h \cap \Omega, \; \mathcal{N}_h^b = \mathcal{N}_h \cap \partial\Omega,\\
&\mathcal{T}_h^i = \{T \in \mathcal{T}_h \mid T \text{ is an interface element}\}.
\end{aligned}$$

For each node $X_i = (x_i, y_i)^t \in \mathcal{N}_h$, we define a global IFE basis function $\Phi_i(X) = \Phi_i(x, y)$ as follows:

- $\Phi_i|_T \in S_h(T), \; \forall T \in \mathcal{T}_h$.
- $\Phi_i(X_j) = \delta_{ij}, \; \forall X_j \in \mathcal{N}_h$.
- Φ_i is continuous at every node $X_j \in \mathcal{N}_h$.

Then we define the IFE space $S_h(\Omega)$ over the whole solution domain as follows:

$$S_h(\Omega) = span\{\Phi_i, i \in \mathcal{N}_h\},$$

where $i \in \mathcal{N}_h$ means $(x_i, y_i) \in \mathcal{N}_h$. We note that every function of $S_h(\Omega)$ satisfies the homogeneous interface jump conditions. Also, for each interface element $T \in \mathcal{T}_h^i$, we use the IFE function $\phi_{T,J}$ to globally define a function $\Phi_{T,J}$ by the usual zero extension outside T. Then, the IFE interpolation discussed in the previous section suggests we look for an IFE solution to the interface problem in the following form:

$$u_h(X) = \sum_{j \in \mathcal{N}_h^o} u_j \Phi_j(X) + \sum_{j \in \mathcal{N}_h^b} g(X_j)\Phi_j(X) + \sum_{T \in \mathcal{T}_h^i} q_T \Phi_{T,J}(X),$$

with coefficient $u_j, j \in \mathcal{N}_h^o$ to be determined, where $g(X)$ is given in the boundary condition (1.2) and q_T is given by (3.23). Finally, using the weak form (4.27), we have the following equations for the IFE solution u_h:

$$\begin{aligned}
&\sum_{j \in \mathcal{N}_h^o} \left(\sum_{T \in \mathcal{T}_h} \int_T \beta \nabla \Phi_i \cdot \nabla \Phi_j dX \right) u_j \\
= \; &\int_\Omega \Phi_i f dX - \int_\Gamma \Phi_i Q ds - \sum_{j \in \mathcal{N}_h^b} \left(\sum_{T \in \mathcal{T}_h} \int_T \beta \nabla \Phi_i \cdot \nabla \Phi_j dX \right) g(X_j) \\
&- \sum_{T \in \mathcal{T}_h^i} q_T \left(\int_T \beta \nabla \Phi_i \cdot \nabla \Phi_{T,J} dX \right), \; \forall i \in \mathcal{N}_h^o.
\end{aligned} \tag{4.28}$$

Remarks:

- If the flux jump $Q = 0$, then the IFE method described by (4.28) reduces to those IFE methods in [15, 32, 31, 33] developed for solving interface problems with homogeneous jump conditions; hence, the new IFE methods presented here are natural extensions of the previous IFE methods.

- Furthermore, we note that the coefficient matrix and the vector corresponding to the first integral on the right hand side of (4.28) are exactly the same as those in the IFE methods for homogeneous jump conditions discussed in [15, 32, 31, 33]. The other three terms on the right hand of (4.28) can be easily implemented through the standard vector assembling procedure in finite element computation.
- All the discussions above can be readily apply to the 1D interface problem (2.5) - (2.8).

We now use numerical examples to demonstrate the convergence of the new IFE methods for solving interface problems with a nonhomogeneous flux jump condition.

IFE solution to the 1D interface problem: We consider applying the new 1D IFE functions to solve the interface problem (2.5) - (2.8) in which f and the boundary conditions are chosen such that its exact solution u is given in (3.24). Also, we assume that the coefficient β and interface location α are as before. Table 4 lists the errors in L^2 and semi-H^1 norms of the IFE solution u_h for this interface problem. The datum in this table obey

$$\|u_h - u\|_0 \approx 7.7582 \times 10^{-2}\ h^{1.9916},\ |u_h - u| \approx 2.7160 \times 10^{-1}\ h^{0.9934}$$

which demonstrate the optimal convergence of the IFE solution.

h	$\|u_h - u\|_0$	$\|u_h - u\|_1$
1/16	3.0784×10^{-4}	1.7139×10^{-2}
1/32	7.7836×10^{-5}	8.7038×10^{-3}
1/64	1.9706×10^{-5}	4.3791×10^{-3}
1/128	4.9804×10^{-6}	2.2083×10^{-3}
1/256	1.2451×10^{-6}	1.1042×10^{-3}
1/512	3.1127×10^{-7}	5.5208×10^{-4}
1/1024	7.7821×10^{-8}	2.7604×10^{-4}

TABLE 4. Errors in the IFE solutions for the 1D interface problem with $\beta^- = 1$ and $\beta^+ = 20000$.

Triangular IFE solution to the 2D interface problem: In this example, we consider using the IFE functions on triangular meshes to solve the interface problem (1.1)-(1.4) to which the exact solution is $u(x, y)$ defined by (3.25). Also, we assume that all the domains and parameters are the same as those in the 2D triangular IFE interpolation example in the previous section. The errors in the L^2 and semi-H^1 norms for the triangular IFE solutions are listed in Table 5 from which we have

$$\|u_h - u\|_0 \approx 3.0268\ h^{2.0431},\ |u_h - u|_1 \approx 7.7877\ h^{1.0087}$$

demonstrating that our triangular IFE method can solve the interface problems with nonhomogeneous flux condition at the optimal convergence rate.

Bilinear IFE solution to 2D interface problems: In this example, we use the bilinear IFE functions to solve the interface problem (1.1)-(1.4) to which the exact solution is $u(x, y)$ defined by (3.26). Again, we assume that all the domains and parameters are the same as those in the 2D rectangular IFE interpolation example in the previous section. Table 6 contains errors of the bilinear IFE solutions u_h with various mesh size h. We can easily see that the datum in the first and second

h	$\|u_h - u\|_0$	$\|u_h - u\|_1$
1/16	9.9678×10^{-3}	4.7479×10^{-1}
1/32	2.7714×10^{-3}	2.3745×10^{-1}
1/64	6.0798×10^{-4}	1.1687×10^{-1}
1/128	1.4727×10^{-4}	5.8104×10^{-2}
1/256	3.6370×10^{-5}	2.9108×10^{-2}

TABLE 5. The errors of the triangular IFE solutions for the 2D interface problem with $\beta^- = 10000$ and $\beta^+ = 10$.

columns of this table satisfy

$$\|u_h - u\|_0 \approx \frac{1}{4} \left\|u_{\hat{h}} - u\right\|_0, \ |u_h - u|_1 \approx \frac{1}{2} \left|u_{\hat{h}} - u\right|_1,$$

for $h = \hat{h}/2$. Using linear regression, we can also see that the data in this table obey

$$\|u_h - u\|_0 \approx 4.1440 \ h^{1.9806}, \ |u_h - u|_1 \approx 8.5601 \ h^{0.9906},$$

which indicate that the bilinear IFE solution u_h converges to the exact solution with convergence rates $O(h^2)$ and $O(h)$ in the L^2 norm and H^1 norm, respectively.

However, numerical experiments indicate that the IFE solution does not always have the second order convergence in the L^∞ norm. For example, the data in the fourth column of Table 6 obey

$$|u_h - u|_\infty \approx 0.2261 \ h^{1.1140}$$

which clearly shows that the rate at which u_h converges to u is not $O(h^2)$. Similar phenomenons have been observed when IFE methods are applied to solve interface problems with homogeneous jump conditions [15, 31]. The question under what conditions the IFE solution can have a second order convergence in the L^∞ norm deserves further investigations.

h	$\|u_h - u\|_0$	$\|u_h - u\|_1$	$\|u_h - u\|_\infty$
1/16	1.8523×10^{-2}	5.5089×10^{-1}	1.2984×10^{-2}
1/32	3.9352×10^{-3}	2.7578×10^{-1}	3.2897×10^{-3}
1/64	1.0293×10^{-3}	1.3888×10^{-1}	2.4211×10^{-3}
1/128	3.0337×10^{-4}	6.9828×10^{-2}	1.0082×10^{-3}
1/256	6.9673×10^{-5}	3.5349×10^{-2}	4.9377×10^{-4}

TABLE 6. The errors of the rectangular IFE solutions for the 2D interface problem with $\beta^- = 1$ and $\beta^+ = 10$.

5. Conclusions

In this paper, we have discussed immersed finite element (IFE) functions that can be used to solve the typical 2nd order elliptic partial differential equations whose discontinuous coefficient leads to a nonhomogeneous flux jump condition. The mesh of these IFE functions can be formed without consideration of the interface location. Our numerical experiments demonstrate that these new IFE functions can approximate functions with a nonhomogeneous flux jump at the optimal convergence rate. We have developed Galerkin methods based on these new IFE functions that can optimally solve the interface problems with a nonhomogeneous flux jump condition. These new IFE methods are natural extensions of those IFE methods

[2, 15, 32, 31, 33] designed for handling homogeneous jump conditions such that the new IFE methods can be easily implemented by adding simple subroutines to the existing codes for the previous IFE methods.

References

[1] S. Adjerid and T. Lin. Higher-order immersed discontinuous Galerkin methods. *Int. J. Inf. Syst. Sci.*, 3(4):555–568, 2007.

[2] S. Adjerid and T. Lin. p-th degree immersed finite element for boundary value problems with discontinuous coefficients. *Appl. Numer. Math*, 59(6):1303–1321, 2009.

[3] I. Babuška. The finite element method for elliptic equations with discontinuous coefficients. *Computing*, 5:207–213, 1970.

[4] I. Babuška, G. Caloz, and J. E. Osborn. Special finite element methods for a class of second order elliptic prolbems with rough coefficients. *SIAM J. Numer. Anal.*, 31:945–981, 1994.

[5] I. Babuška and J. E. Osborn. Finite element methods for the solution of problems with rough input data. In P. Grisvard, W. Wendland, and J.R. Whiteman, editors, *Singular and Constructive Methods for their Treatment, Lecture Notes in Mathematics, #1121*, pages 1–18, New York, 1985. Springer-Verlag.

[6] J. H. Bramble and J. T. King. A finite element method for interface problems in domains with smooth boundary and interfaces. *Adv. Comput. Math.*, 6:109–138, 1996.

[7] A. Bernardo, A. Marquez and S. Meddahi, Analysis of an interaction problem between an electromagnetic field and an elastic body, International Journal of Numerical Analysis and Modeling, Vol 7, No 4 (2010) 749-765.

[8] B. Camp, T. Lin, Y. Lin, and W. Sun. Quadratic immersed finite element spaces and their approximation capabilities. *Adv. Comput. Math.*, 24(1-4):81–112, 2006.

[9] Z. Chen and J. Zou. Finite element methods and their convergence for elliptic and parabolic interface problems. *Numer. Math.*, 79:175–202, 1998.

[10] D.M. Cook. *The Theory of the Electromagnetic Field*. Prentice-Hall, Englewood Cliffs, 1975.

[11] R. E. Ewing, Z. Li, T. Lin, and Y. Lin. The immersed finite volume element methods for the elliptic interface problems. Modelling '98 (prague). *Math. Comput. Simulation*, 50(1-4):63–76, 1999.

[12] A. L. Fogelson and J. P. Keener. Immersed interface methods for neumann and related problems in two and three dimensions. *SIAM J. Sci. Comput.*, 22:1630–1654, 2001.

[13] Y. Gong, B. Li, and Z. Li. Immersed-interface finite-element methods for elliptic interface problems with non-homogeneous jump conditions. *SIAM J. Numer. Anal.*, 46:472–495, 2008.

[14] X.-M. He. Bilinear immersed finite elements for interface problems. *Ph.D. dissertation, Virginia Polytechnic Institute and State University*, 2009.

[15] X.-M. He, T. Lin, and Y. Lin. Approximation capability of a bilinear immersed finite element space. *Numer. Methods Partial Differential Equations*, 24(5):1265–1300, 2008.

[16] X.-M. He, T. Lin, and Y. Lin. A bilinear immersed finite volume element method for the diffusion equation with discontinuous coefficients. *Commun. Comput. Phys.*, 6(1):185–202, 2009.

[17] B. Heinrich. *Finite Difference Methods on Irregular Networks*, volume 82 of *International Series of Numerical Mathematics*. Birkhäuser, Boston, 1987.

[18] D. W. Hewitt. The embedded curved boundary method for orthogonal simulation meshes. *J. Comput. Phys.*, 138:585–616, 1997.

[19] D. M. Ingram, D. M. Causon, and C. G. Mingham. Developments in Cartesian cut cell methods. *Math. Comput. Simulation*, 61(3-6):561–572, 2003.

[20] K. Ito, Z. Li, and Y. Kyei. Higher-order, cartesian grid based finite difference schemes for elliptic equations on irregular domains. *SIAM J. Sci. Comput.*, 27(1):346–367, 2005.

[21] H. Ji, F.-S. Lien, and E. Yee. An efficient second-order accurate cut-cell method for solving the variable coeffcient poisson equation with jump conditions on irregular domains. *International Journal for Numerical Methods in Fluids*, 52:723–748, 2006.

[22] B. Jovanovic and L. Vulkov, Numerical solution of a two-dimensional parabolic transmission problem, International Journal of Numerical Analysis and Modeling, Vol 7, No 1 (2010) 156-172.

[23] J. Karatson and S. Korotov, Discrete maximum principles for FEM solutions of some nonlinear elliptic interface problems, International Journal of Numerical Analysis and Modeling, Vol 6, No 1 (2009) 1-16.

[24] R. Kafafy, T. Lin, Y. Lin, and J. Wang. Three-dimensional immersed finite element methods for electric field simulation in composite materials. *Int. J. Numer. Meth. Engrg.*, 64(7):940–972, 2005.

[25] R. Kafafy, J. Wang, and T. Lin. A hybrid-grid immersed-finite-element particle-in-cell simulation model of ion optics plasma dynamics. *Dyn. Contin. Discrete Impuls. Syst. Ser. B Appl. Algorithms*, 12:1–16, 2005.
[26] D. V. Le, B. C. Khoo, and J. Peraire. An immersed interface method for viscous incompressible flows involving rigid and flexible boundaries. *J .Comput. Phys.*, 220(6):109–138, 2006.
[27] R. J. LeVeque and Z. Li. The immersed interface method for elliptic equations with discontinuous coefficients and singular sources. *SIAM J. Numer. Anal.*, 34:1019–1044, 1994.
[28] Z. Li. The immersed interface method using a finite element formulation. *Applied Numer. Math.*, 27:253–267, 1998.
[29] Z. Li and K. Ito. Maximum principle preserving schemes for interface problems with discontinuous coefficients. *SIAM J. Sci. Comput.*, 23:339–361, 2001.
[30] Z. Li and K. Ito. *The immersed interface method: Numerical solutions of PDEs involving interfaces and irregular domains*, volume 33 of *Frontiers in Applied Mathematics*. SIAM, Philadelphia, PA, 2006.
[31] Z. Li, T. Lin, Y. Lin, and R. C. Rogers. An immersed finite element space and its approximation capability. *Numer. Methods Partial Differential Equations*, 20(3):338–367, 2004.
[32] Z. Li, T. Lin, and X. Wu. New Cartesian grid methods for interface problems using the finite element formulation. *Numer. Math.*, 96(1):61–98, 2003.
[33] T. Lin, Y. Lin, R. C. Rogers, and L. M. Ryan. A rectangular immersed finite element method for interface problems. In P. Minev and Y. Lin, editors, *Advances in Computation: Theory and Practice, Vol. 7*, pages 107–114. Nova Science Publishers, Inc., 2001.
[34] T. Lin, Y. Lin, and W. Sun. Error estimation of a class of quadratic immersed finite element methods for elliptic interface problems. *Discrete Contin. Dyn. Syst. Ser. B*, 7(4):807–823, 2007.
[35] T. Miyazaki. *Water Flow In Soils*. Taylor & Francis, Boca Raton, 2nd edition, 2006.
[36] M. Overmann and R. Klein. A cartesian grid finite volume method for elliptic equations with variable coefficients and embedded interfaces. *J .Comput. Phys.*, 219:749–769, 2006.
[37] A. A. Samarskiĭ and V. B. Andreev. *Méthods aux Différences pour Équations Ellipticques*. Mir, Moscow, 1978.
[38] S. A. Sauter and R. Warnke. Composite finite elements for elliptic boundary value problems with discontinuous coefficients. *Computing*, 77(1):29–55, 2006.
[39] J. Wang, D. Kondrashov, P. Liewer, and S. Karmesin. Three-dimensional particle simulation modeling of ion propulsion plasma environment for deep space 1. *J. Spacecraft & Rockets*, 38(3):433–440, 2001.
[40] J. Wang, J. Polk, J. Brophy, and I. Katz. 3-d particle simulations of nstar ion optics plasma flow. In *IEPC 2001-085*, 2001.
[41] T. S. Wang. A Hermite cubic immersed finite element space for beam design problems. Master's thesis, Virginia Polytechnic Institute and State University, U. S. A, 2005.
[42] H. Xie, Z. Li and Z. Qiao, A finite element method for elasticity interface problems with locally modified triangulations, International Journal of Numerical Analysis and Modeling, Vol 8, No 2 (2011) 189-200.
[43] K. Zhang and S. Wang, A computational scheme for option under jump diffusion processes, International Journal of Numerical Analysis and Modeling, Vol 6, No 1 (2009) 110-123.
[44] Y. C. Zhou and G. W. Wei. On the fictitious-domain and interpolation formulations of the matched interface and boundary (MIB) method. *J. Comput. Phys*, 219(1):228–246, 2006.
[45] Y. C. Zhou, S. Zhao, M. Feig, and G. W. Wei. High order matched interface and boundary method for elliptic equations with discontinuous coefficients and singular sources. *J. Comput. Phys*, 213(1):1–30, 2006.

Department of Mathematics and Statistics, Missouri University of Science and Technology, Rolla, MO 65409
E-mail: hex@mst.edu

Department of Mathematics, Virginia Tech, Blacksburg, VA 24061
E-mail: tlin@math.vt.edu

Department of Applied Mathematics, Hong Kong polytechnic University, Hung Hom, Hong Kong, and Department of Mathematical and Statistics Science, University of Alberta, Edmonton AB, T6G 2G1, Canada
E-mail: yanlin@ualberta.ca